

Online Monitoring for Safe Pedestrian-Vehicle Interactions

Peter Du, Zhe Huang[†], Tianqi Liu[†], Ke Xu[†], Qichao Gao[†], Hussein Sibai,
 Katherine Driggs-Campbell, Sayan Mitra
 University of Illinois at Urbana-Champaign

{peterdu2,zheh4,tliu51,kexu6,qgao10,sibai2,krdc,mitras}@illinois.edu

July 21, 2022

Abstract

As autonomous systems begin to operate amongst humans, methods for safe interaction must be investigated. We consider an example of a small autonomous vehicle in a pedestrian zone that must safely maneuver around people in a free-form fashion. We investigate two key questions: How can we effectively integrate pedestrian intent estimation into our autonomous stack? Can we develop an online monitoring framework to give formal guarantees on the safety of such human-robot interactions? We present a pedestrian intent estimation framework that can accurately predict future pedestrian trajectories given multiple possible goal locations. We integrate this into a reachability-based online monitoring scheme that formally assesses the safety of these interactions with nearly real-time performance (approximately 0.3s). These techniques are integrated on a test vehicle with a complete in-house autonomous stack, demonstrating effective and safe interaction in real-world experiments.

1 Introduction

Autonomous systems are quickly entering human dominated fields in the form of drones and self-driving cars, and becoming tangible technologies that will impact the human experience. As these systems begin to share space and operate among humans, safety becomes a primary concern [5, 17]. Despite many successful demonstrations of autonomous driving, safe interaction between autonomous vehicles and other road users remains an open problem [36, 9, 12].

We consider two key factors currently impeding safe interactive autonomy. First, designing interactive controllers that consider predictions about human movement remains a challenge due to the high variability in human behavior [11]. Second, providing formal guarantees for autonomous systems is challenging due to complexities introduced by many intertwined modules in the autonomous stack as well multi-agent interactions [20].

One test case where this is particularly obvious is an autonomous shuttle scenario; where an autonomous vehicle operates on small roads and sidewalks and may encounter pedestrians through free-form interaction. Such automated systems have been developed for campus settings [32, 38] and pedestrian zones [14, 24]. These systems typically require and have heuristic decision-making for determining safe interaction (e.g., if an obstacle is within some preset distance, stop [28]). One common “lesson learned” is that interacting with pedestrians is difficult due to their unpredictability [38, 37]. As pedestrians are vulnerable agents and have very few constraints on their motion,

determining methods for safe interaction is both critical for reducing risk of accidents and improving efficiency by limiting over-conservative performance. Further, many studies state that an on-board safety driver or watchdog is necessary to monitor the system operation [38, 24].

In this work, we present an initial foray into integrating human motion prediction with an autonomous system’s decision and control framework as well as an online monitoring system. Leveraging data-driven verification approaches to provide formal guarantees, we demonstrate how DryVR, an offline reachability tool for hybrid dynamical systems [16], can be used in an online setting to give a formal assessment of safety as the autonomous vehicle drives in close proximity to a human. In short, we present the following contributions:

1. *Intent estimation.* We present a particle filter-based approach to predict human motion and provide future trajectories as well as estimate the likelihood over multiple goals for each agent.
2. *Safety monitoring.* We extend offline reachability techniques to an online setting. This near-realtime monitoring approach allows us to use forward reachable sets to dynamically assess safety.
3. *System integration.* We demonstrate the feasibility of our efforts on a complete autonomous system which includes lane detection, pedestrian tracking and intent prediction, localization, lane-tracking control, tactical decision-making, and an online monitoring module.

The paper is organized as follows. In Section 2, we present a literature review of works related to modeling pedestrian intent and online monitoring, as applied to autonomous systems. Then, we present an overview of our experimental platform and our in-house autonomous stack in Section 3. In Sections 4 and 5, we present our methodology for pedestrian intent estimation and online monitoring via reachability. We conclude with an analysis of our integrated system and discuss our findings and future directions in Sections 6 and 7.

2 Background

We present a brief literature review of techniques for modeling pedestrian interactions for use in decision-making and control frameworks as well as verification methods to provide guarantees for autonomous systems.

2.1 Pedestrian Modeling

There are three main techniques used to predict pedestrian trajectories: data-driven approaches like neural networks, decision-making approaches like Markov models, and tracking or filter-based approaches like Kalman filters. Alahi et al. [1] formulated pedestrian behavior modeling as a sequential prediction task, adding a social pooling layer to the LSTM (Long Short Term Memory Network) architecture to capture the interaction between humans in crowded scenarios. Yi et al. [39] encoded pedestrian behavior into sparse displacement volumes, which are used as input and output of the Behavior-CNN they proposed.

Karasev et al. [22] used a jump-Markov process to model pedestrian behavior, which assumes that the goal is slowly time-varying and that the pedestrians are rational: meaning they will only slightly deviate from the optimal trajectory that minimizes the path’s cost. The authors define intent as a policy in a Markov decision process, which is solved as an optimal control problem

incorporating uncertainty through a stochastic Boltzmann policy. Ikeda et al. [21] use the concept of sub-goals from cognitive science, which assumes that pedestrians reach the final destination by walking through a sequence of sub-goals. The sub-goals are estimated by discretizing the environment and learning the transition probabilities between sub-goals based on observed trajectories.

Schneider and Gavrilu [33] used an Extended Kalman Filter to conduct a comparative study between single dynamic models and Interacting Multiple Models which combine multiple motion patterns. Kooij et al. [23] represent pedestrian behaviors as a switched linear dynamical system with constant position and constant velocity. A Dynamic Bayesian Network is implemented to encode context cues such as a pedestrian’s heading and the distance between a vehicle and pedestrian.

2.2 Reachability

The problem of checking whether a model of a cyber-physical system reaches a set of unsafe states starting from a set of initial states, is usually posed as *reachability* problem of a hybrid automaton [4, 35, 25], and this problem is generally *undecidable* [34]. Restricting the reachability question, for example, to finite time horizons, or allowing false-positives in the answers, leads to *semi-decidable* problems. However, until recently, the semi-decision procedures available scaled poorly in terms of both running times and memory usage. Through a series of conceptual and algorithmic breakthroughs and discovery of clever data structures, CPS verification has made astonishing progress: Using the support functions data structure, the SpaceEX tool [18] can perform reachability analysis of linear hybrid systems with dozens of continuous dimensions. More recently, the HyLAA tool [6, 7] has been reported to have successfully verified models with more than 10,000 dimensions exploiting sparse dynamics and generalized star set data structures. Verification of nonlinear models with dozens and even hundreds of dimensions is now routinely achieved with tools like C2E2 [13, 15], Flow* [10], and CORA [3].

In terms of autonomous vehicle applications, a remarkable study has been the demonstration of the feasibility of online verification for automatic lane change maneuvers on a Cadillac SRX at the Robotics Institute of Carnegie Mellon University [2]. The analysis was performed with linearized approximations of the vehicle dynamics relative to all possible behaviors surrounding cars. Although our online monitor is also based on reachability analysis, our controller uses pedestrian intentions and network-based lane detection modules. Further, our data-driven reachability analysis approach is directly applicable to nonlinear vehicle models where as [2] utilizes a linearized model. Finally, although the computing cycles available on the Cadillac SRX are not discussed in [2], we note that our on-board computers running vision, positioning, and estimation algorithms severely constrained the network bandwidth and the cycles available for monitoring.

3 Autonomous Vehicle Platform

We describe our autonomous testbed in terms of the experimental hardware and the software components used in our autonomous stack.

3.1 Vehicle Hardware and Experimental Setup

Our vehicle is a Polaris GEM electric car outfitted with sensing and computing hardware by AutonomouStuff (Figure 2). The on-board computers include an embedded PC with a sixth Generation Intel i7-6700 2.4 GHz quad-core CPU, NVIDIA GeForce GTX 1050 GPU with 2GB of

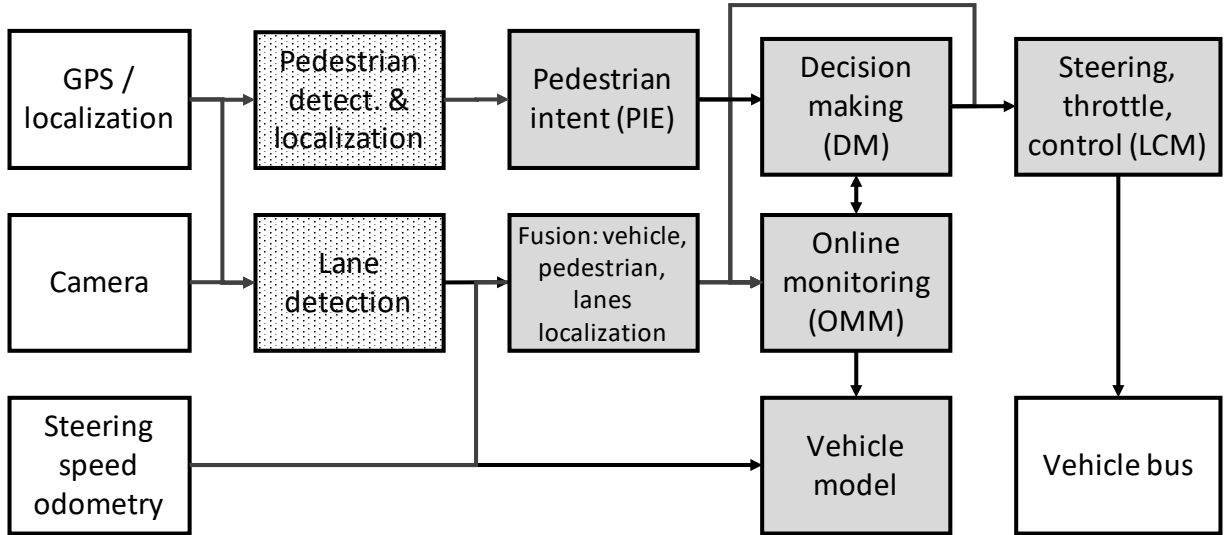


Figure 1: System architecture. The dark gray modules constitute the key contributions of this work the light gray modules are built using YOLOv3 [31] and LaneNet [27].

GDDR5, and two laptops each with an eighth Generation Intel i7-8750H 2.2 GHz six-core CPU, NVIDIA GeForce RTX 2060 GPU with 6GB of GDDR5. The sensors include a Velodyne LIDAR, a Radar, GPS & Inertial Measurement Units, and a single Mako G-319C forward facing camera.

Our experimental arena is a 3,000 sq. ft. indoor open research space with marked lanes. We implemented a localization protocol that gives global coordinates of the vehicle using Decawave ultra-wideband beacons and time-of-flight calculations. Decawave DW1000 ICs were used which provide a 2D localization accuracy within around 20 cm. Message error rates for the DW1000 do not exceed 10% and in our testing, we saw failure rates less than one per minute with position data frame rates of around 3 fps. Our indoor testing facility was unobstructed by walls and allowed for a clear line of sight among the Decawave chips.

3.2 Lane detection

The goal of the lane detection module is to observe the presence of a lane in an RGB input image and output an annotated image with the curvature of the lane and the vehicle offset from the lane’s center. By transforming this annotated image to a *birds-eye view (BEV)* using the vehicle’s position information, we obtain the lane’s position and geometry information in a global coordinate frame. To achieve this we used LaneNet, a deep neural network based method for lane detection [27].

LaneNet consists of an encoder-decoder stage, a binary semantic segmentation branch, and an instance semantic segmentation branch that uses a discriminative loss function for semantic segmentation used in post-processing. In the segmentation branch, the neural network runs a binary classifier on pixels and creates a binary lane mask. The embedding branch creates an instance segmentation and assigns a lane ID to each pixel while ignoring background ones.

To fully utilize the results from the deep neural network, an image that combines the extracted features from each LaneNet branch needs to be generated. Canny edge detection is used to extract the feature from lane instance segmentation [8]. It generates an image of lane boundaries which



Figure 2: Autonomous Vehicle Testing Platform. (a) Picture of the AutonomouStuff GEM in the testing arena. (b) Lane detection using a modified LaneNet. *Left*: Binary lane mask generated by LaneNet binary semantic segmentation branch. *Middle*: Lane instance segmentation generate by LaneNet embedding branch. *Right*: Combined closing image of the binary lane mask and instance image. (c) *Left*: A polynomial fit (green) of the pixels associated with the left (blue) and right (red) lane on bird’s-eye view image. *Right*: Annotated lane detection output image with estimated offset. (d) Object detection and localization public road sample, with vehicle in blue, pedestrian in red and positions in yellow. (e) Object detection and localization sample at the test arena, with pedestrian in red and positions in yellow.

is then overlaid on the binary lane segmentation to give a combined image of two neural network branches. A morphological operation is then applied to strengthen the features of the combined image.

A histogram of the bottom half of the BEV of the combined image is calculated and used to partition the image into horizontal slices. The image is then split into two parts vertically and a sliding window method applied on each part to find left and right lane pixels. With groups of pixels as either the left lane or the right lane, we fit a polynomial to each group and output the estimation of lanes (see Figure 2). The curvature of the lane and vehicle offset from the center of the lane is calculated according to the predicted polynomial and the vehicle localization data.

3.3 Pedestrian detection and localization

The pedestrian detection and the Decawave localization module takes the position/heading of the car and video from the camera to produce an estimated position of a pedestrian in the current video frame in the global coordinate system.

We use YOLOv3 for implementing this module [31]. For an input image from the camera video, the network divides it into an $S \times S$ coarse grid of smaller sub-images. For each of these sub-images, the network detects the presence of objects and places bounding boxes around them. In our experiments, we only process objects from a few classes such as pedestrians, vehicles, traffic signs, etc.

To locate the position of detected pedestrian, we first estimate the focal length of the camera by placing objects of known dimension at different distances from the camera. We then use the size of the detected bounding box, the estimated focal length of the camera, and the assumed width of the pedestrians (0.47 meters) to estimate the distance (y -coordinate) of the pedestrian from the vehicle. We further utilize the pixel-to-meter ratio for an object with assumed width to estimate the horizontal deviation (x -coordinate). The resulting system is able to perform pedestrian detection and localization at 13 fps with a mean error less than one meter. The estimated x and y -coordinates are then converted from ego-vehicle coordinates to the global coordinate frame using position data from vehicle localization.

4 Autonomy modules

We present our approaches for estimating pedestrian intent and predicting their future trajectories as well as online monitoring via our reachability framework.

4.1 Pedestrian Intent Estimation (*PIE*) Module

The pedestrian intent module takes a pedestrian position measurement in the global coordinate frame from the pedestrian detection & localization module and produces a future trajectory that ends at a predefined goal state. The predicted pedestrian trajectory is fed into the decision-making and online reachability modules to assess the safety of the current driving scenario.

The estimation algorithm assumes that the map information and all possible pedestrian intents are given as a set of possible goal locations. For example, in a crosswalk scenario, the pedestrian typically has two possible intents. One is to go across the road, which is represented by an intent on the other side of the road. The other is to go along the road, for which the intent can be set as a location on the same side of the road as the pedestrian. Based on the assumption, the sequential measurement of the pedestrian motion is used to predict its intent during run-time.

An accurate pedestrian model is necessary to predict the pedestrian intent. The Generalized Potential Field Approach (GPFA) is used to model the pedestrian behavior [30]. A set of sources are created to represent the obstacles in the map and to generate the repulsive force on the pedestrian, while a sink is set at the intent location to attract the pedestrian. The sum of forces is the acceleration, which is the control input u_t to the state space model of the pedestrian, giving the following dynamical model:

$$\begin{aligned}x_t &= Fx_{t-1} + Gu_{t-1} + w_t \\y_t &= Hx_{t-1} + v_t\end{aligned}\tag{1}$$

where F is the state transition matrix, G is the control matrix, and x_t is the state vector of the pedestrian, which is the location and the velocity at time t . H is the measurement matrix and y_t is the measurement of pedestrian location. It is assumed that the process noise w_t and the measurement noise v_t are Gaussian white noise.

As the transition model involves highly nonlinear GPFA, we employ a Multi-hypothesis Particle Filter to estimate the likely intent [29]. Initially, each particle sampled will be assigned a hypothesis on pedestrian intent I_i . The number of intents N considered in this paper is three, corresponding to either crossing the lane or heading along the lane in either direction. The probability of assigning different intents to a particle is the same, as $1/N_I$ for each intent. In the prediction step, each particle predicts the pedestrian position at the next time stamp based on the hypothesis of the intent to which it is assigned. In the update step, the weights of particles are updated based on the deviation of the position prediction from the measurement.

In contrast to the method presented in [29], the weights of particles with the same intent hypothesis are summed to generate the probability distribution of different intents at that time stamp. Sequential importance re-sampling is implemented after the weights are updated. The intent with the highest probability is chosen to create the trajectory of the pedestrian in the future using GPFA based on the current measured position. It was mentioned in [29] that the re-sampling step was not needed due to the robustness requirement for changes of the true intent of the pedestrian. However, no re-sampling being involved would make the intent estimation vulnerable to sample degeneracy, i.e. only few particles with significant weights are kept throughout the intent estimation process, which leads to the loss of population nature of the particle filter. In fact, sequential

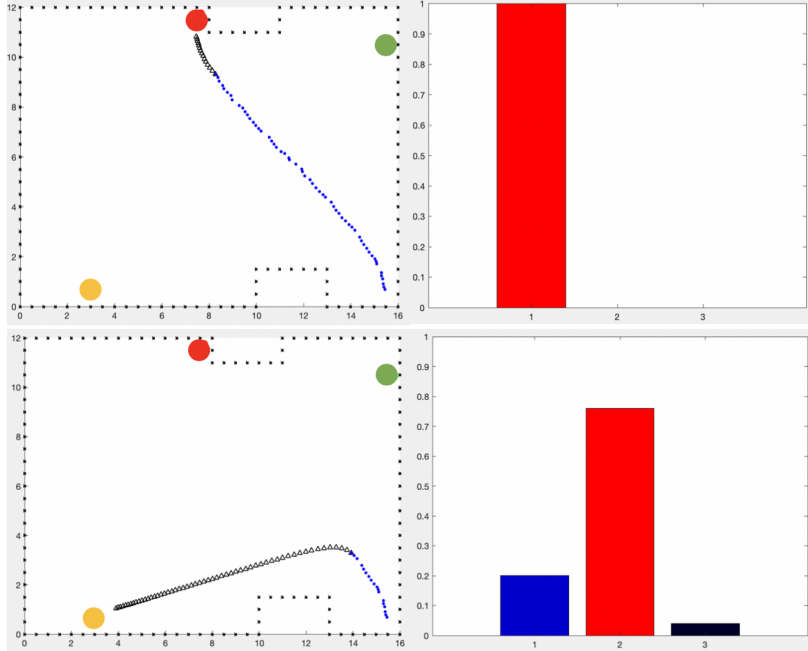


Figure 3: Two sample outputs of pedestrian intent estimation for scenario with three goals. *Left*: Predicted trajectories. *Right*: Probability distribution of pedestrian intents.

importance re-sampling makes use of the quantity of particles to inherit the probability distribution inferred from the last round and causes no harm to the algorithm robustness. Another difference is that though many of the model parameters are the same as in [30, 29], no additional noise is manually added due to the sensor noise inherent in the measurement. For online performance, we initially generate 200 particles for each intent (600 total).

Ultimately, this module produces the estimated pedestrian trajectory as a sequence of location-time pairs $\tau = \{\langle p_1, t_1 \rangle, \dots, \langle p_k, t_k \rangle\}$, where the final point is estimated goal location. The algorithm runs at 5 Hz, which is sufficient for the online monitoring application. Figure 3 shows the algorithm performance on a data sample from a public dataset [26]. There are three possible intents in this case (the red as No. 1, the yellow as No. 2 and the green as No. 3), which are surrounded by black star walls. The pedestrian trajectory is the blue dots and the trajectory prediction is represented by the black triangles. Our methodology is well tuned and validated on this public dataset [26], accurately predicting the intent and effectively yielding the future trajectory.

4.2 Decision Module

The *Decision Module (DM)* takes as input the estimated pedestrian trajectories generated by the pedestrian intent estimation (*PIE*) module, the current state of the vehicle, and decides whether the vehicle should continue at the current speed (*go*), slow down (*slow*), or quickly stop (*brake*).

The *DM* makes the following assumptions: (1) a pair of left and right lane markers are accurately detected and localized by the lane detection module (Section 3.2). The mid-lane curve is represented by a fixed sequence of points $\{\ell_1, \dots, \ell_L\}$ in the plane. (2) The time horizon of the pedestrian trajectory estimate τ is long enough relative to the initial position of the pedestrian, so that it intersects the mid-lane iff it enters the region between the lanes. (3) The control module (*LCM*)

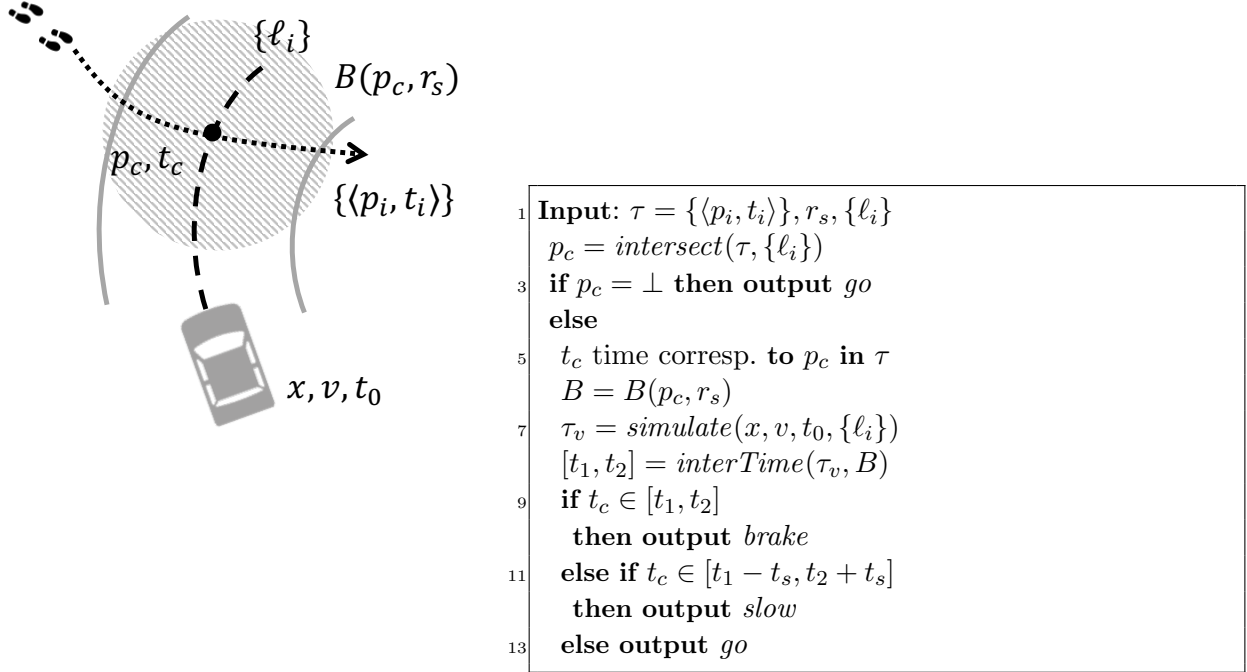


Figure 4: Decision-Making Module. *Left:* Schematic illustration of decision making module. *Right:* Decision module pseudocode.

ensures that the vehicle keeps the vehicle centered between the lanes with its heading aligned with the tangent of the mid-lane curve.

The heuristic we have implemented in the *DM* roughly works as follows (see Figure 4).¹ Suppose the computation starts at time t_0 . Recall that a pedestrian trajectory estimate is represented by a sequence of location-time pairs $\tau = \{\langle p_1, t_1 \rangle, \dots, \langle p_k, t_k \rangle\}$, with the interpretation that the pedestrian is expected to be at location p_i at time t_i . From a given pedestrian trajectory estimate τ and a given mid-lane curve $\{\ell_i\}$, first a point of intersection (p_c) of the lane and pedestrian is computed. If no such point exists, then *DM* returns *go*. This action is a safe decision because by Assumption (2), if the pedestrian’s intent enters the lanes then it also intersects the mid-lane. If there is an intersection p_c , then let t_c be the time of intersection of τ with the mid-lane. Let B be a ball of radius r_s centered at p_c , where r_s is a safety radius computed based on the geometry of the vehicle. Then, *DM* simulates the vehicle forward from its current position (x), velocity (v), time (t_0), assuming that the *LCM* makes it follow the mid-lane, generating a vehicle trajectory τ_v . Next, the time interval $[t_1, t_2]$ is computed that over-approximates the duration that τ_v is B .

If t_c is contained in $[t_1, t_2]$, that is, the vehicle and the pedestrian are simultaneously within B , then the decision is *brake*. If t_c is in the bigger interval $[t_1 - t_s, t_2 + t_s]$ then the decision is *slow*, otherwise the decision is *go*. Under the assumptions stated above and large enough values of t_s, r_s (depending on x, v, τ), elementary calculations show that the vehicle maintains space from the pedestrian up to time t_k .

¹ We acknowledge that the decision module described here is simplistic and that there are many more advanced approaches we could use. While we hope to explore this in future work, we note that the contributions of this paper are (1) integrating novel pedestrian models and (2) develop an online monitoring scheme for a *given* autonomous system.

Our actual implementation generalizes the above basic strategy along several dimensions. It handles multiple pedestrian trajectory estimates from the *PIE*; it can simulate the vehicle forward with more realistic *LCM*'s that possibly violate Assumption (3); and instead of working with exact intersections it works with distances and intervals. Finally, the strategy could be used as a building block to implement a *risk-sensitive* decision module that associates different trajectory estimates (τ) and safety radii (r_s) to calculate the expected risk of different decisions.

Our algorithm has $O(m + n)$ time complexity and $O(m + n)$ space complexity, in which m is the size of pedestrian intent estimations and n is the size of pre-recorded locations of points on the center of the lane. In our experiments, *DM* takes about 1.2 ms to evaluate the current situation, which makes it possible to be used as an online module on any autonomous vehicle.

4.3 Velocity and Lane Tracking Control

We use a control module to generate speed and steering commands to navigate the vehicle autonomously. The control module is integrated into our ROS framework to interface with the other modules of the GEM vehicle platform as well as the PACMod drive-by-wire system. Separate controllers maintain the vehicle at a desired speed (set by the user) and adjust steering angle such that the vehicle follows a given lane. PID controllers are used in both cases. The inputs to the control module include:

- *lane center deviation* — from lane detection
- *stop and go command* — from decision module
- *vehicle speed* — from drive-by-wire system

To achieve lane tracking, the PID steering controller uses the deviation from lane center (in meters) outputted by the lane detection module. The deviation is treated as an error signal and the controller applies steering inputs to track a zero error reference.

Vehicle speed control is done in a similar fashion. The PID speed controller reads the current vehicle velocity and acceleration commands are generated to track a constant speed set by the user. The speed controller has different operating modes which depend on the output of the decision module (DM). When the DM decides the current situation is safe, the controller will track a constant velocity as described previously. If the DM decides the situation is unsafe and outputs *brake*, the controller will immediately brake, overriding any previous acceleration command.

5 Online Monitoring Module (*OMM*)

For online safety or risk monitoring, the estimated current states of the vehicle and the pedestrian(s) must be computed forward in time to check for possible loss of separation. This is an instance of the *reachability analysis problem* which is the cornerstone of formal verification [4, 19]. Thus far most applications of reachability for robotic and cyber-physical systems have been for offline design verification. For online monitoring, reachability analysis must be: (1) *accurate*—to reduce false positives, and (2) *quick*—to allow for timely recovery and mitigating actions, if needed. Specifically, for a 4-6 second look-ahead horizon (trajectory estimate) the reachability analysis has to finish within 10-100 milliseconds. Making the problem harder, the initial position estimates have uncertainty from the localization (see Sec. 3.1), and there may be multiple pedestrian and vehicle

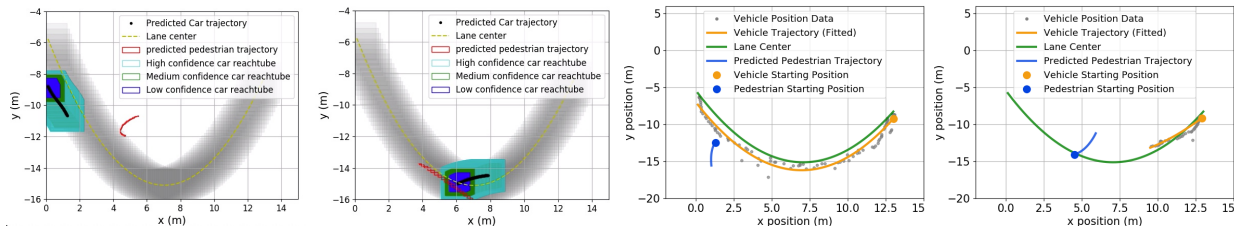


Figure 5: Example results from left to right: (1) Vehicle and pedestrian reachtubes for scenario where the decision module deemed the system to be safe and no collision will occur. (2) Vehicle and pedestrian reachtubes for scenario where the decision module deemed the system to be unsafe with the predicted pedestrian trajectory crossing the vehicle’s path. (3) Vehicle and pedestrian traces for scenario where the decision module deemed the system to be safe and no collision will occur. Vehicle is able to complete entire path without stopping. (4) Vehicle and pedestrian traces for scenario where the decision module deemed the system to be unsafe with the predicted pedestrian trajectory crossing the vehicle’s path. Vehicle stops and waits for pedestrian to clear.

trajectories to propagate forward. Current offline reachability algorithms for hybrid systems can work in minutes for 6-12-dimensional nonlinear models. Thus, for scalable online monitoring, a 3 order of magnitude improvement in verification technology is needed. In this paper, we identify a restricted class of scenarios and for those we show how this can be achieved in our *OMM*.

Given a hybrid or a dynamical system \mathcal{A} over a state space \mathcal{X} , a set of initial states $\Theta \subseteq \mathcal{X}$, and a time horizon $T > 0$, a state $\mathbf{x} \in \mathcal{X}$ is reachable if there exists an execution of \mathcal{A} starting from Θ , of duration at most T , that reaches \mathbf{x} . The set of reachable states is written as $\text{Reach}_{\mathcal{A}}(\Theta, T) \subseteq \mathcal{X}$. Our design of *OMM* uses the data-driven reachability approach as implemented in the DryVR [15] and C2E2 [13] tools. Roughly speaking, simulation data generated from a model or an executable for \mathcal{A} , is used together with sensitivity analysis of \mathcal{A} to compute over-approximations of $\text{Reach}_{\mathcal{A}}(\Theta, T)$. If the intersection $R \cap U$ of such an over-approximation $R \supseteq \text{Reach}_{\mathcal{A}}(\Theta, T)$ and an unsafe set U , is empty then the *OMM* can safely decide that system is safe up to time T . On the other hand, if $R \cap U \neq \emptyset$ then *OMM* cannot infer that there necessarily exists an unsafe execution. In this case, the algorithm splits Θ in to smaller regions and computes $\text{Reach}_{\mathcal{A}}(\cdot, T)$ over-approximations from each of those partitions. This step is called *refinement*. Certain special properties of sensitivity functions ensure that this process converges to $\text{Reach}_{\mathcal{A}}(\Theta, T)$, but this splitting can lead to exponentially many computations, and is the leading contributor to the slowdown of reachability analysis. In our implementation of this algorithm in the *OMM*, we introduce the notion of a *partitioning budget*, which restricts the number of partitions of Θ . By controlling this quantity,

For our experiments we use a simplified 5-dimensional dynamical model of the car:

$$\dot{x} = v \cos \theta, \dot{y} = v \sin \theta, \dot{\phi} = u, \dot{v} = a, \dot{\theta} = \frac{v}{L} \tan(\phi)$$

where u is the input steering angular velocity and a is the input acceleration, (x, y) is the position, v is the speed, and θ is the steering angle, ϕ is its heading angle and L is the length of the car. The overall system \mathcal{A} used for reachability analysis is the composition of this vehicle model with the *LCM* of Section 4.3. We used DryVR to learn the sensitivity function for this model offline.

There are several sources of errors and uncertainties in measuring the initial state Θ of the above systems. For example, the position of the car and the pedestrian have uncertainties arising

from the localization system. We define a nested sequence of hyperrectangular initial sets $\Theta_1 \subset \Theta_2 \subset \dots \Theta_k$ —with increasing levels of confidence and looser error bounds. For each Θ_i we compute corresponding over-approximations of $\text{Reach}_{\mathcal{A}}(\Theta_i, T)$ using DryVR starting from Θ_k . From the monotonicity of the $\text{Reach}_{\mathcal{A}}()$ it follows that $\text{Reach}_{\mathcal{A}}(\Theta_1, T) \subseteq \text{Reach}_{\mathcal{A}}(\Theta_2, T) \subseteq \dots \text{Reach}_{\mathcal{A}}(\Theta_k, T)$, and therefore, if $\text{Reach}_{\mathcal{A}}(\Theta_i, T)$ is verified safe then so are the smaller sets. Thus, if $\text{Reach}_{\mathcal{A}}(\Theta_i, T)$ is verified safe then the computation stops. Further, When computing any of these tubes, we set the number of refinements according to the partition budget. Implementing these strategies with a look-ahead time of $t = 5$ seconds gave us a maximum verification time of 0.6 seconds on the vehicle’s computers. This shows the promise of our approach particularly because our current implementation of *OMM* does not yet exploit parallelism of the algorithm nor availability of GPUs.

6 Experimental Results

To demonstrate our complete pipeline (with off the shelf components and in-house autonomous modules), we run our autonomous system in two test cases. Figure 5 show examples of the our integrated system. The two graphs on the right show vehicle and pedestrian trajectories during two different scenarios. The two graphs on the left show the outputs of the reachability analysis in two other scenarios. In all cases, as the vehicle comes around the curved lane in the test arena, a pedestrian is detected and tracked.

The *PIE* estimates the goal location and passes the predicted trajectory to the DM. In Figure 5 (3), the predicted trajectory shows the pedestrian walking away from the lane without intersecting the vehicle’s path. As a result, the vehicle proceeds to safely move past the pedestrian without braking at any point during the experiment. In Figure 5 (4), the predicted trajectory suggests that the pedestrian will cross the lane. The DM decides this situation is unsafe as a collision is likely and signals the controller to brake. The vehicle thus stops before completing its path and waits for the pedestrian to clear.

The *OMM* gets estimates of pedestrian intent and vehicle state, performs reachability analysis to infer whether the system is safe up to a look-ahead time T . As discussed earlier, the state estimates have large and fluctuating errors and we use nested uncertainty bounds with different levels of confidence. In our experiments, for a look-ahead time of $T = 5$ seconds, this computation along with safety checking with estimated pedestrian trajectory, finished on average in less than 0.3 seconds. The tube in Figure 5 (2), although it intersects the predicted pedestrian trajectory, it shrinks in size which means that the car is braking. With fixed look-ahead time ($T = 5$ seconds), a small $\text{Reach}_{\mathcal{A}}(\Theta, T)$ in position space (x, y) implies that the car is moving slowly. In Figure 5 (1), the car reachtube does not intersect the pedestrian trajectory, it does not brake and the tube is longer. Using reachability analysis, *OMM* alerted the vehicle in scenarios where the *DM* missed the danger of collision as the latter uses a single simulation to make decisions.

Increasing the number of tubes with different initial sets with different confidence levels or allowing refinements can give more precise monitoring. However, for short intervals of time and using reliable sensors, this level of computation is time efficient and accurate enough to oversee the decisions of the vehicle.

7 Discussion

We present an integrated autonomous system that uses a novel pedestrian intent estimator to safely maneuver amongst humans. We add another layer of safety and risk assessment by developing a reachability-based online monitoring scheme that formally assesses the safety of these interactions with nearly real-time performance ($\sim 0.5s$). These techniques are integrated on a test vehicle with a complete in-house autonomous stack, demonstrating effective and safe interaction in real-world experiments.

In our current experiments, we make many assumptions and control many aspects of the system to ensure the baseline performance is functional. However, in reality, any of the submodules may fail. For example, we only tested scenarios where the *PIE* correctly predicted the pedestrian. Given that no model can perfectly predict a human, we hope to explore scenarios where the prediction is incorrect, making the need for an online monitor more pressing. We note that similar statements hold for the vision and decision-making modules. We also found that timing and synchronizing the components was difficult and had a noticeable impact on the safety assessment, both from the decision-making and online monitoring perspective. We hope to include such inaccuracies and uncertainties in future iterations of our online monitor.

Acknowledgement

We thank AutonomousStuff (now part of Hexagon) for providing the vehicle platform used in this work. We are grateful to David Young for software development and management and to John Hart for support with safety procedures and training.

References

- [1] A. Alahi, K. Goel, V. Ramanathan, A. Robicquet, L. Fei-Fei, and S. Savarese. Social lstm: Human trajectory prediction in crowded spaces. In *Proceedings of the IEEE conference on computer vision and pattern recognition*, pages 961–971, 2016.
- [2] M. Althoff and J. M. Dolan. Online verification of automated road vehicles using reachability analysis. *IEEE Trans. Robotics*, 30(4):903–918, 2014.
- [3] M. Althoff and D. Grebenyuk. Implementation of interval arithmetic in CORA 2016. In *Proc. of the 3rd International Workshop on Applied Verification for Continuous and Hybrid Systems*, pages 91–105, 2016.
- [4] R. Alur, C. Courcoubetis, N. Halbwachs, T. A. Henzinger, P.-H. Ho, X. Nicollin, A. Olivero, J. Sifakis, and S. Yovine. The algorithmic analysis of hybrid systems. *Theoretical Computer Science*, 138(1):3–34, 1995.
- [5] A. Bajcsy, S. L. Herbert, D. Fridovich-Keil, J. F. Fisac, S. Deglurkar, A. D. Dragan, and C. J. Tomlin. A scalable framework for real-time multi-robot, multi-human collision avoidance. *arXiv preprint arXiv:1811.05929*, 2018.

- [6] S. Bak and P. S. Duggirala. Hylaa: A tool for computing simulation-equivalent reachability for linear systems. In *Proceedings of the 20th International Conference on Hybrid Systems: Computation and Control*, pages 173–178. ACM, 2017.
- [7] S. Bak, H. Tran, and T. T. Johnson. Numerical verification of affine systems with up to a billion dimensions. In *Proceedings of the 22nd ACM International Conference on Hybrid Systems: Computation and Control, HSCC 2019, Montreal, QC, Canada, April 16-18, 2019.*, pages 23–32, 2019.
- [8] J. Canny. A computational approach to edge detection. *IEEE Trans. Pattern Anal. Mach. Intell.*, 8(6):679–698, June 1986.
- [9] B. Chen, D. Zhao, and H. Peng. Evaluation of automated vehicles encountering pedestrians at unsignalized crossings. In *IEEE Intelligent Vehicles Symposium (IV)*, pages 1679–1685, 2017.
- [10] X. Chen, E. brahm, and S. Sankaranarayanan. Flow*: An analyzer for non-linear hybrid systems. In N. Sharygina and H. Veith, editors, *Computer Aided Verification*, volume 8044 of *Lecture Notes in Computer Science*, pages 258–263. Springer Berlin Heidelberg, 2013.
- [11] K. Driggs-Campbell, R. Dong, and R. Bajcsy. Robust, informative human-in-the-loop predictions via empirical reachable sets. *IEEE Transactions on Intelligent Vehicles*, 3(3):300–309, 2018.
- [12] K. Driggs-Campbell, V. Govindarajan, and R. Bajcsy. Integrating intuitive driver models in autonomous planning for interactive maneuvers. *IEEE Transactions on Intelligent Transportation Systems*, 18(12):3461–3472, 2017.
- [13] P. S. Duggirala, S. Mitra, and M. Viswanathan. Verification of annotated models from executions. In *EMSOFT*, 2013.
- [14] G. Eden, B. Nanchen, R. Ramseyer, and F. Evéquo. On the road with an autonomous passenger shuttle: Integration in public spaces. In *CHI Extended Abstracts on Human Factors in Computing Systems, CHI EA '17*, pages 1569–1576, New York, NY, USA, 2017. ACM.
- [15] C. Fan, B. Qi, and S. Mitra. Data-driven formal reasoning and their applications in safety analysis of vehicle autonomy features. *IEEE Design & Test*, 35(3):31–38, 2018.
- [16] C. Fan, B. Qi, S. Mitra, and M. Viswanathan. Data-driven verification and compositional reasoning for automotive systems. In *Computer Aided Verification*, pages 441–461. Springer International Publishing, 2017.
- [17] J. F. Fisac, A. Bajcsy, S. L. Herbert, D. Fridovich-Keil, S. Wang, C. J. Tomlin, and A. D. Dragan. Probabilistically safe robot planning with confidence-based human predictions. *arXiv preprint arXiv:1806.00109*, 2018.
- [18] G. Frehse, C. L. Guernic, A. Donzé, S. Cotton, R. Ray, O. Lebeltel, R. Ripado, A. Girard, T. Dang, and O. Maler. SpaceEx: Scalable verification of hybrid systems. In G. Gopalakrishnan and S. Qadeer, editors, *Computer Aided Verification*, volume 6806 of *Lecture Notes in Computer Science*, pages 379–395. Springer, 2011.

- [19] A. Girard. Reachability of uncertain linear systems using zonotopes. In *International Workshop on Hybrid Systems: Computation and Control*, pages 291–305. Springer, 2005.
- [20] V. Govindarajan, K. Driggs-Campbell, and R. Bajcsy. Data-driven reachability analysis for human-in-the-loop systems. In *2017 IEEE 56th Annual Conference on Decision and Control (CDC)*, pages 2617–2622. IEEE, 2017.
- [21] T. Ikeda, Y. Chigodo, D. Rea, F. Zanlungo, M. Shiomi, and T. Kanda. Modeling and prediction of pedestrian behavior based on the sub-goal concept. *Robotics*, 10, 2013.
- [22] V. Karasev, A. Ayvaci, B. Heisele, and S. Soatto. Intent-aware long-term prediction of pedestrian motion. In *2016 IEEE International Conference on Robotics and Automation (ICRA)*, pages 2543–2549. IEEE, 2016.
- [23] J. F. P. Kooij, N. Schneider, F. Flohr, and D. M. Gavrilu. Context-based pedestrian path prediction. In *European Conference on Computer Vision*, pages 618–633. Springer, 2014.
- [24] R. Kümmerle, M. Ruhnke, B. Steder, C. Stachniss, and W. Burgard. Autonomous robot navigation in highly populated pedestrian zones. *Journal of Field Robotics*, 32(4):565–589, 2015.
- [25] J. Lygeros, K. H. Johansson, S. N. Simic, J. Zhang, and S. S. Sastry. Dynamical properties of hybrid automata. *IEEE Transactions on automatic control*, 48(1):2–17, 2003.
- [26] B. Majecka. Edinburgh informatics forum pedestrian database. URL: <http://homepages.inf.ed.ac.uk/rbf/FORUMTRACKING>, 2010.
- [27] D. Neven, B. D. Brabandere, S. Georgoulis, M. Proesmans, and L. V. Gool. Towards end-to-end lane detection: an instance segmentation approach. *2018 IEEE Intelligent Vehicles Symposium (IV)*, pages 286–291, 2018.
- [28] S. Nordhoff, J. de Winter, R. Madigan, N. Merat, B. van Arem, and R. Happee. User acceptance of automated shuttles in berlin-schöneberg: A questionnaire study. *Transportation Research Part F: Traffic Psychology and Behaviour*, 58:843–854, 2018.
- [29] F. Particke, M. Hiller, C. Feist, and J. Thielecke. Improvements in pedestrian movement prediction by considering multiple intentions in a multi-hypotheses filter. In *2018 IEEE/ION Position, Location and Navigation Symposium (PLANS)*, pages 209–212. IEEE, 2018.
- [30] F. Particke, L. Patino-Studencki, J. Thielecke, and C. Feist. Pedestrian tracking using a generalized potential field approach. In *VISIGRAPP (6: VISAPP)*, pages 509–514, 2017.
- [31] J. Redmon and A. Farhadi. Yolov3: An incremental improvement. *arXiv preprint arXiv:1804.02767*, 2018.
- [32] P. Rodríguez. *Safety of pedestrians and cyclists when interacting with automated vehicles a case study of the WEpods*. PhD thesis, Master thesis, TU Eindhoven, 2017.
- [33] N. Schneider and D. M. Gavrilu. Pedestrian path prediction with recursive bayesian filters: A comparative study. In *German Conference on Pattern Recognition*, pages 174–183. Springer, 2013.

- [34] T. A. Henzinger and P. -H. Ho. Algorithmic analysis of nonlinear hybrid systems. In P. Wolper, editor, *Proceedings of the 7th International Conference On Computer Aided Verification*, volume 939, pages 225–238, Liege, Belgium, 1995. Springer Verlag.
- [35] P. Tabuada. *Verification and Control of Hybrid Systems: A Symbolic Approach*. Springer Publishing Company, Incorporated, 1st edition, 2009.
- [36] S. M. Thornton, F. E. Lewis, V. Zhang, M. J. Kochenderfer, and J. C. Gerdes. Value sensitive design for autonomous vehicle motion planning. In *IEEE Intelligent Vehicles Symposium (IV)*, pages 1157–1162, 2018.
- [37] E. Trulls, A. Corominas Murtra, J. Pérez-Ibarz, G. Ferrer, D. Vasquez, J. M. Mirats-Tur, and A. Sanfeliu. Autonomous navigation for mobile service robots in urban pedestrian environments. *Journal of Field Robotics*, 28(3):329–354, 2011.
- [38] J. W. Van der Wiel. Automated shuttles on public roads: Lessons learned, 2017.
- [39] S. Yi, H. Li, and X. Wang. Pedestrian behavior understanding and prediction with deep neural networks. In *European Conference on Computer Vision*, pages 263–279. Springer, 2016.